Modified adaptive algebraic tomographic reconstruction of gas distribution from incomplete projection by a two-wavelength absorption scheme

Ning Li (李 宁)* and Chunsheng Weng (翁春生)

State Key Laboratory of Transient Physics, Nanjing University of Science and Technology, Nanjing 210094, China

**Corresponding author: lining@mail.njust.edu.cn*

Received November 22, 2010; accepted January 20, 2011; posted online April 29, 2011

A modified adaptive algebraic reconstruction technique (MAART) with an auto-adjustment relaxation parameter and smoothness regularization is developed to reveal the tomographic reconstruction of H_2O distribution in combustion from incomplete projections. Determinations of relaxation parameter and regularization factor are discussed with regard to the consideration of improvement in reconstruction and reduction of computational burden. A two-wavelength scheme from tunable diode laser absorption measurement, 7444.36 and 7185.59 cm^{-1}, is used to simplify the nonlinear solution problem for obtaining the tomographic distributions of concentration and temperature simultaneously. Results of calculations demonstrate that MAART can perform the reconstruction results more efficiently with little complex modification and much lower iterations as compared with the traditional algebraic reconstruction technique (ART) or simultaneous iterative reconstruction technique (SIRT) methods. The stability of the algorithm is studied by reconstruction from projections with random noise at different levels to demonstrate the dependence of reconstruction results on precise line-of-sight measurements.

OCIS codes: 120.0120, 110.0110, 300.0300.

doi: 10.3788/COL201109.061201.

The technology with tunable diode laser absorption spectroscopy shows great potential for application in the measurement of gas concentration and temperature during combustion[1−4], as well as measurement of distribution in the line-of-sight nonuniform-property flows[5−7]. The tunable diode laser sensing is a technology that is quite attractive from the perspective of practical applications with regard to the robustness of the system, relative ease of use, and reasonable cost. Fiber lasers can easily cover the extended range of specific transitions for more number of species by the wavelength division multiplexing (WDM) technique. However, the inherent characteristic of tunable diode laser sensing makes it more difficult to achieve spatially resolved measurements. The optical scanning system and reconstruction algorithm need to be considered for the reconstruction of the gas concentration and temperature distributions with reasonable projections. Unlike the rotating computed tomography (CT) employed in medical radiation dosimetry[8], the laser source and detector arrays with fixed positions are designed to maintain the time resolution for dynamic combustion measurement, and this leads to incomplete projections from the limited optics arrangement.

Tomography reconstruction is a nonlinear optimization problem, attributed to the nonlinear temperature dependence on absorption coefficients. An increase in transitions would be an effective way to extend the absorption information for better quality of reconstruction[9]. Techniques of simulated annealing (SA) have been investigated for reconstruction of temperature and concentration from 20 projection locations with 10 wavelengths at each location in the 10 × 10 grids. However, when the number of limited projections is much lower than the number of unknown variables, derivation of the solution for an ill-posed matrix equation by similar methods becomes unfeasible. Algebraic methods have been shown to provide better reconstructions from limited views, albeit with the disadvantage of a greater computational burden. An algebraic reconstruction technique (ART) has been discussed in gas tomography reconstruction where a total of 400 projections were collected from four beam platforms (a single platform was rotated to produce a fan beam) to reconstruct the gas distribution in the 10 × 10 grids[10]. In this letter, we discuss a modified adaptive algebraic reconstruction technique (MAART), which introduces adaptive adjustment of relaxation parameters[11] and smoothness regularization during the reconstruction procedure. This technique is developed to reconstruct the distributions of concentration and temperature simultaneously under incomplete projections for fast computation and high quality.

A scanning geometry measurement of parallel laser-detector pairs at multi-view with a fixed location was investigated in the region of interest, which was divided into 8 × 8 discretization grids. The projection views were arranged equally in a range of 180° with an angle interval

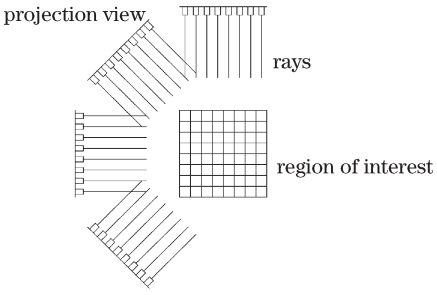

Fig. 1. Optical arrangement for multi-view parallel scanning geometry ($V = 4$, $R = 8$).

Table 1. Spectroscopic Parameters of H_2O Utilized in This Letter

Wavelength (cm^{-1})	Line Strength ($cm^{-1}\cdot$ atm^{-1})	Lower State Energy (cm^{-1})
7185.59	1.97×10^{-2}	1045.1
7444.35	5.4×10^{-4}	1774.8
7444.37 (Overlapped)	5.76×10^{-4}	1806.7

of $180°/V$, where V is the number of projection views. In each projection view, the laser array was equally spaced along a straight line with a length interval of L/R, where L is the length of the reconstructed region and R is the number of rays in a single view. Two wavelengths were scanned at each projection by wavelength multiplexing. The number of variables involved in the reconstruction is 128, comprising the 64 unknown temperature variables and 64 unknown concentration variables.

The Beer-Lambert law governing gas absorption spectroscopy for narrow-linewidth laser radiation through an absorbing medium and the two-wavelength scheme are used in this study to extend the absorption information in a single projection and, further, to infer concentration and temperature by the tunable diode laser sensing technology[5]. H_2O was treated as the attractive combustion species to be monitored because of its widespread absorption transitions, which exist in the near-infrared range, and its indication function for combustion efficiency as a primary product in hydrocarbon combustion. Diode lasers and detectors are inexpensive and robust for industrial application within 1–2 μm. Two transitions, 7444.36 and 7185.59 cm^{-1}, have been proved to maintain suitable line-strength and to be free of significant interference from nearby transitions. Table 1 presents relative spectroscopic parameters of transitions obtained from the HITRAN2000 database. The lower energy state between transitions is sufficiently different to yield a line-strength ratio that is sensitive to the temperature being probed between 1000–2000 K, as shown in Fig. 2.

Asymmetric H_2O temperature and concentration distribution models were created by superimposing two Gaussian peaks on a paraboloid to simulate the combustive conditions encountered in practice, as depicted in Fig. 3.

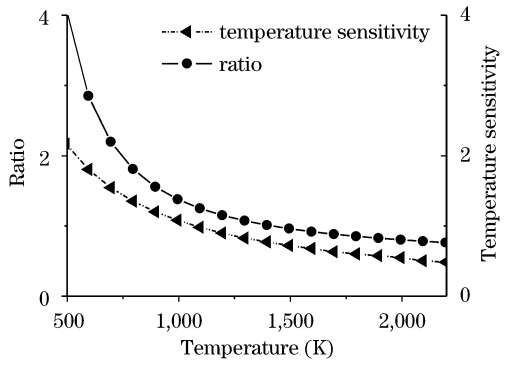

Fig. 2. Calculated ratio and temperature sensitivity of selected transitions.

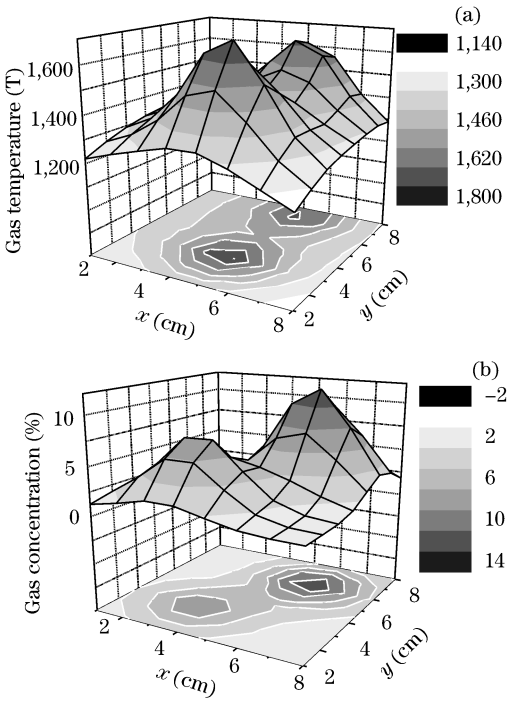

Fig. 3. Phantoms for (a) temperature and (b) concentration distribution.

A line-of-sight absorption measurement was performed along the ray, and the integrated absorbance across a specific spectral line could be written as a discretization expression:

$$A_{vi,j} = \sum_{n=1}^{N}\sum_{m=1}^{M}[PS(T)X]_{vi,(m,n)}\,L_{(m,n),j} = \sum_{n=1}^{N}\sum_{m=1}^{M}\alpha_{vi,(m,n)}L_{(m,n),j} \quad (j=1,2,\cdots,J), \tag{1}$$

where j is the index of the ray, and J is the total number of rays from all the views, m and n are the indices of row and column in the grid with size given by $M \times N$. A_{vi} denotes the integrated absorbance across the transition at the wavelength v_i. $L_{(m,n),j}$ is the length of the path in the grid (m,n) through which the ray j passes. The absorption coefficient $\alpha_{vi,(m,n)}$, containing the parameters of transition line-strength $S_{vi}(T)$, gas molar fraction of the absorbing species X, and total pressure of gas P, was calculated in all the grids according to the tomography algorithm at two independent wavelengths in a measure to infer the unknown temperature and concentration of the gas. Application of the ART method solves linear Eq. (1) in iterative equations as follows:

$$\alpha^{k}_{vi,(m,n)} = \alpha^{k-1}_{vi,(m,n)} + \lambda\Big(\sum_{n=1}^{N}\sum_{m=1}^{M}\alpha^{k-1}_{vi,(m,n)}L_{(m,n),j} - A_{vi,j}\Big), \tag{2}$$

where k is the iteration index in the ART procedure, and λ is the relaxation parameter, which represents the contribution of the absorption at grid (m,n) to the integral of ray j. The reconstruction is terminated when

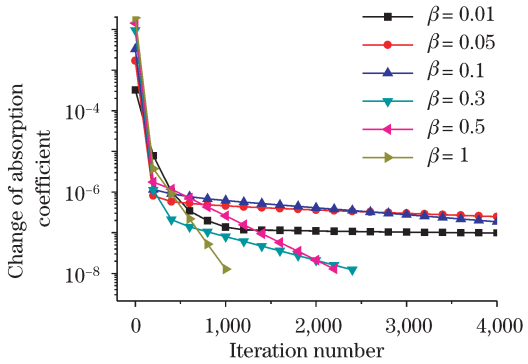

Fig. 4. Convergence speed versus iteration at different parameter β (V=4, R=8, 0.5% noise levels in projections).

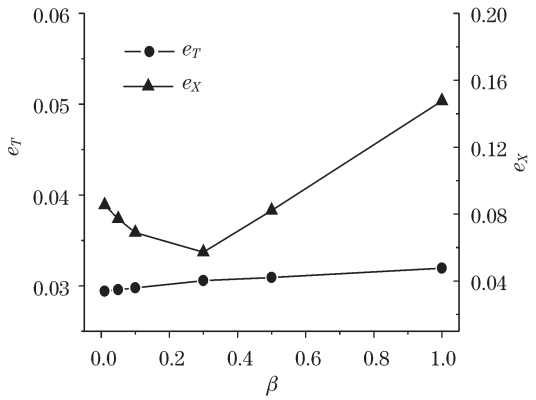

Fig. 5. Effect of β in relaxation parameter on reconstruction errors of e_T and e_X by MAART (V=4, R=8, 0.5% noise levels in projections).

the change of absorption coefficient in Eq. (2) becomes less than 1×10^{-9} between two consecutive iterations. The quality of reconstructed results for distributions of both concentration and temperature was evaluated by the normalized mean absolute error:

$$e_X = \frac{\sum_{n=1}^{N}\sum_{m=1}^{M}\left|X_{m,n}^{\mathrm{cal}} - X_{m,n}^{\mathrm{pha}}\right|}{\sum_{n=1}^{N}\sum_{m=1}^{M}\left|X_{m,n}^{\mathrm{pha}}\right|},$$
$$e_T = \frac{\sum_{n=1}^{N}\sum_{m=1}^{M}\left|T_{m,n}^{\mathrm{cal}} - T_{m,n}^{\mathrm{pha}}\right|}{\sum_{n=1}^{N}\sum_{m=1}^{M}\left|T_{m,n}^{\mathrm{pha}}\right|}, \quad (3)$$

where e_T and e_X are the normalized mean absolute errors between reconstructed and phantom values for concentration and temperature, $X_{m,n}^{\mathrm{cal}}$ and $T_{m,n}^{\mathrm{cal}}$ represent the reconstructed concentration and temperature distributions for the grid (m,n), and $X_{m,n}^{\mathrm{pha}}$ and $T_{m,n}^{\mathrm{pha}}$ represent concentration and temperature distributions in the phantom, respectively.

It is evident that the contribution of the absorption at grid (m,n) is not only dependent on the length of the path, but also on the corresponding gas concentration, temperature (and the pressure, which is uniform in the present case). Unlike the conventional ART method, the

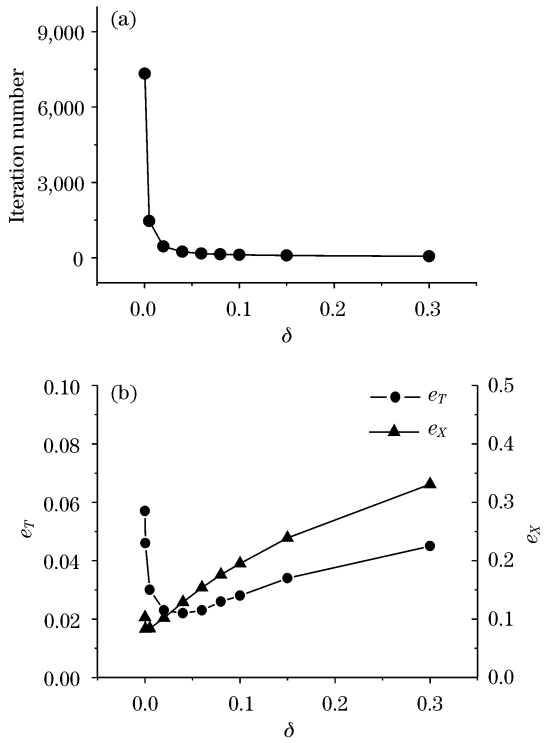

Fig. 6. Effect of regularization factor δ on (a) iteration number and (b) reconstruction errors of e_T and e_X by MAART (V=4, R=8, 0.5% noise levels in projections).

relaxation parameter in the MAART method is automatically changed during the reconstruction procedure, and the larger contribution of absorption to the ray integral would have a larger adjustment step during the iteration:

$$\lambda = \beta \times (\alpha_{vi,(m,n)}^{k-1} L_{ij}) / (\sum_{n=1}^{N}\sum_{m=1}^{M} \alpha_{vi,(m,n)}^{k-1} L_{(m,n),j}), \quad (4)$$

where β is a constant during the procedure of calculation. This adaptive adjustment of relaxation parameters leads not only to speedy convergence but also to a high-quality reconstruction. The plot of the convergence speed versus iteration at different parameters of β is shown in Fig. 4.

The plot with a small parameter β ($\beta < 0.5$) exhibits an obvious L-shaped curve with a distinct corner. The MAART algorithm works with high efficiency before the corner; thereafter, the convergence speed slows down until the change of absorption coefficient reaches 1×10^{-9}. The computation, approximately 64,593 iterations for a β parameter of 0.01, decreases rapidly with a larger β parameter, to approximately 11,275 iterations for a β parameter of 0.1. Further increase in β would reduce the computation at the cost of degrading the reconstruction quality of gas distribution due to the over-adjustment in iteration, as shown in Fig. 5. The β value, in this instance, would be recommended for selection from 0.1 to 0.3, and correspond to 0.029−0.031 for e_T and 0.068−0.057 for e_X; in addition, the computation is modest as compared with Fig. 4.

Smoothness regularization is established based on the fact that distributions of temperature and concentration should be continuous; further, the values are to be restricted within a reasonable range for specific applica-

tion in practice. The smoothness regularization, which reduces discrepancy between the value of each image grid and its nearest neighbors, is provided as

$$\alpha_{vi,(m,n)}^{k} = (1-\delta) \times \alpha_{vi,(m,n)}^{k-1} + \delta \times \Big(\sum_{y=n-1}^{n+1} \sum_{x=m-1}^{m+1} \alpha_{vi,(x,y)}^{k-1} / 8 \Big), \quad (5)$$

where (x,y) is not equal to (m,n). The absorption coefficient $\alpha_{vi,(m,n)}$ is restricted within $[0, \alpha_{vi}^{\max}]$ during iterations, and $\alpha_{vi}^{\max}$ represents the possible theoretical maximum value of the absorption coefficient in the grids. With regard to the physical meaning of this factor, the value of δ would be selected between 0 and 1, where 0 indicates that no smooth regularization is utilized and 1 indicates that the value of the specific grid is completely dependent on its nearest neighbors. Figure 6 depicts the effect of δ on the speed and quality of reconstruction.

The introduction of δ into the algorithm creates significant advantages for improving the computational efficiency and results of reconstruction. Figure 6 clearly shows the extremely rapid reduction in computation, with the iteration number decreasing from 14,432 to 446 with δ increasing from 0 to 0.02. The influence of further increase in δ on reconstruction computations is not obvious. The effect of the regularization factor δ on results of reconstruction is summarized in Fig. 6 by presenting e_T and e_X of the reconstructions at noise levels of 1%, and the optimal regularization factors for e_T and e_X are 0.03 and 0.01, respectively. It is apparent that, with a larger value of δ, the program would make the reconstructed distribution flat and ignore the variable feature in each grid.

In practice, the numbers of projection views and rays

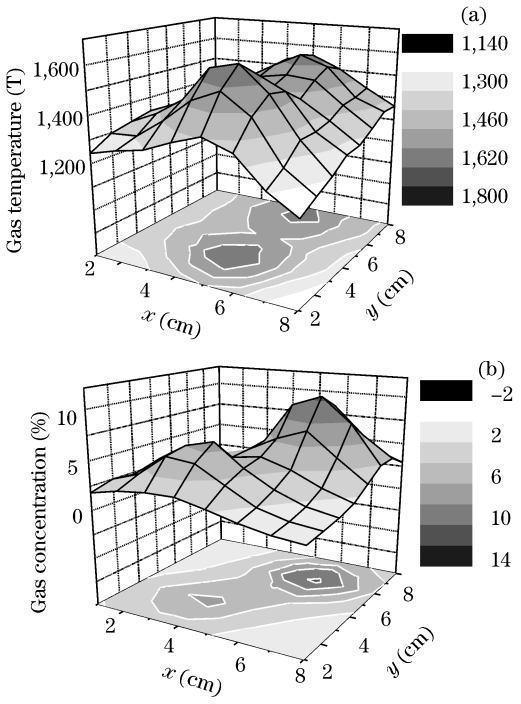

Fig. 7. Reconstructed distributions of (a) temperature and (b) concentration distribution (V=4, R=8, 0.5% noise levels in projections).

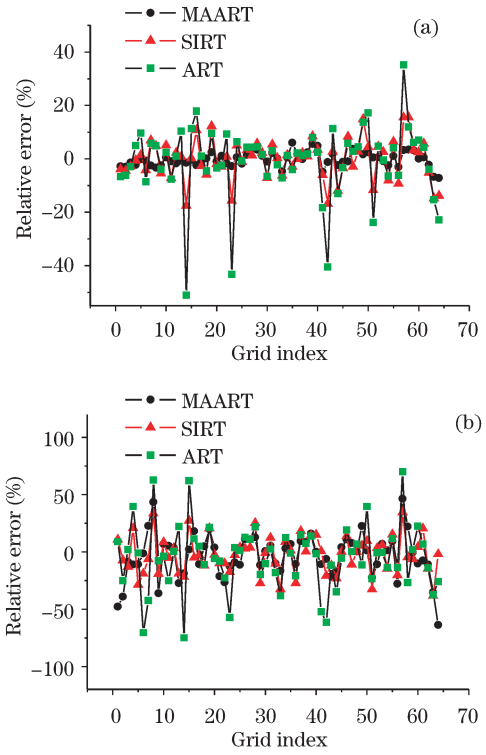

Fig. 8. Comparison of relative errors in (a) temperature and (b) concentration reconstruction from computation by MMART, SIRT, and ART (V=4, R=8, 1% noise levels in projections).

are expected to be minimized with the aim of obtaining a reconstruction of gas distribution that is of satisfying quality. In this study, the four views and eight rays are specified such that this optical arrangement can be easily designed to simplify the configuration of the optical system and to reduce the cost of equipments. Although the total projections of 32 for each wavelength are much lower than the number of unknown variables, the MAART can restrict e_T and e_X within 0.011 and 0.058, respectively. From Fig. 7, it can be seen that the appearance and location of multiple peaks in both temperature and concentration phantoms are reconstructed with excellent agreement. The absolute error of the reconstruction of temperature is less than 89 K, and the error of the reconstruction of concentration is less than 0.013. Most of the deviation points are located in the grids where peaks exist in the phantom; this indicates that the reconstruction would smoothen the peak by the algorithm with a correction of values in the neighboring grids; however, these would, in turn, reduce the fluctuation in the margin of the reconstructed region where fewer laser rays can pass through the corresponding grids. This feature would be extremely attractive in an optical arrangement of fewer views and rays.

A comparison of reconstructions by conventional ART, simultaneous iterative reconstruction technique (SIRT), and MAART is provided in Fig. 8 to explain the feature of the algorithm. In general, the MAART demonstrates satisfying performance for both reconstruction results and computation. The distribution of gas can be obtained after 309 iterations, with $e_T = 0.022$ and $e_X = 0.115$. The SIRT performs the same reconstruction

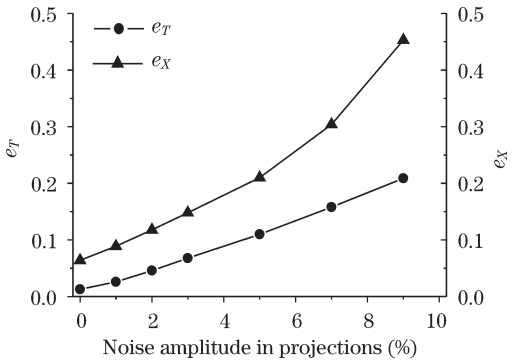

Fig. 9. Effect of random noise in projections on reconstruction errors of e_T and e_X (V=4, R=8).

and obtains similar results with $e_T = 0.057$ and $e_X = 0.12$, which is slightly less optimal than MAART, at the cost of significantly increased computational expenditure of 17,286 iterations. The ART completes the reconstruction in 8,977 interations, yields $e_T = 0.088$ and $e_X = 0.15$. In particular, the errors in the grids at the margin of the reconstructed region are often found to be intolerable. The fluctuation in the absorption coefficient for reconstruction in the margin of the reconstructed region would be significant if fewer laser rays pass through the corresponding grids and if various noises exist. Regularization would be an effective method to suppress artificial value and to ensure that the reconstruction errors remain within a reasonable range.

Simulations are performed to analyze the stability of reconstruction of the MAART method when measured projections contain different levels of noise. Random white noises, with levels ranging from 0% to 10%, are added into the collected projections to simulate the measured signals in practice; the corresponding e_T and e_X are obtained from the reconstructed results, as shown in Fig. 9. Every point in the figure is conducted from 10 times of average calculation of reconstruction containing different random noise distributions at the same level. The e_T value remains close to 0.026 while e_X remains less than 0.089 at a noise level of 1%, which represents the exact line-of-sight measurement with small noise. At noise levels of up to 3%, when measurement is subject to normal noise source, e_T and e_X are close to 0.068 and 0.148, respectively. MAART exhibits better performance in the reconstruction of concentration distribution than in reconstruction of temperature distribution. The reconstruction of temperature is more sensitive to noise in projections due to its nonlinear dependence on the absorption coefficient, as mentioned previously. When the line-of-sight tunable diode laser sensing measurement is carried out in harsh environments with noise levels up to 7%, more views or rays should be considered to provide sufficient projections for better reconstruction results. For example, e_T and e_X are reduced to 0.101 and 0.211 at $V = 4$ and $R = 16$, which correspond to $e_T = 0.158$ and $e_X = 0.304$ at $V = 4$ and $R = 8$.

In conclusion, we propose MAART to realize tomographic reconstruction of H_2O distribution by tunable diode laser sensing using a two-wavelength scheme. The feature of relaxation parameter with auto-adjustment in iteration and smoothness regularization facilitates ascertaining of accurate reconstruction results by MAART with a much lower calculation burden as compared with the conventional ART and SIRT methods, subject to the condition of limited projections. A phantom of H_2O distribution in combustion is utilized to verify the effectiveness of the MAART method and the corresponding optical arrangement. Two transitions, 7,444.36 and 7,185.59 cm^{-1}, have been selected to provide independent absorption information to infer gas concentration and temperature simultaneously; this can be attained while maintaining a suitable temperature sensitivity in the range of 1,000–2,000 K. Appropriate values of β in the relaxation parameter and the regularization factor δ would improve the efficiency of the MAART algorithm as well as the reconstruction quality, as compared with the conventional ART and SIRT methods. The stability of the procedure is analyzed by reconstruction from projections, with incomplete projections at different noise levels. This method would be beneficial in the solving of the nonlinear optimization problem during reconstruction of temperature and concentration distributions by tunable diode laser absorption spectroscopy.

This work was supported by the Young Scientists Fund of the National Natural Science Foundation of China (No. 11002074), the Specialized Research Fund for the Doctoral Program of Higher Education of China (No. 20093219110037), the China Postdoctoral Science Foundation (No. 20100481147), the Jiangsu Planned Projects for Postdoctoral Research Funds (No. 0902094C), and the Nanjing University of Science and Technology Research Funding (No. 2010ZYTS092).

References

1. H. Teichert, T. Fernholz, and V. Ebert, Appl. Opt. **42,** 2043 (2003).
2. S. Zhang, W. Liu, Y. Zhang, X. Shu, D. Yu, R. Kan, J. Dong, H. Geng, and J. Liu, Chin. Opt. Lett. **8,** 443 (2010).
3. J. J. Nikkari, J. M. Di Iorio, and M. J. Thomson, Appl. Opt. **41,** 446 (2002).
4. Y. Gérard, R. J. Holdsworth, and P. A. Martin, Appl. Opt. **46,** 3937 (2007).
5. S. T. Sanders, J. Wang, J. B. Jeffries, and R. K. Hanson, Appl. Opt. **40,** 4404 (2001).
6. X. Liu, J. B. Jeffries, and R. K. Hanson, AIAA Journal **45,** 411 (2007).
7. X. Zhou, X. Liu, J. B. Jeffries, and R. K. Hanson, Meas. Sci. Technol. **14,** 1459 (2003).
8. N. Krstajić and S. J. Doran, Phys. Med. Biol. **52,** N257 (2007).
9. L. Ma and W. Cai, Appl. Opt. **47,** 3751 (2008).
10. N. Li and C. Weng, Chinese J. Lasers (in Chinese) **37,** 1310 (2010).
11. W. Lu and F.-F. Yin, Med. Phys. **31,** 3222 (2004).